NIR Imaging: Development of Digital Image Processing Algorithm for Vein Contrast Enhancement

Nikita V. Remizov*, Denis S. Yakimenko, and Dmitry N. Artemyev
Samara National Research University, 34 Moskovskoye shosse, Samara 443086, Russian Federation
*e-mail: erenv97@yandex.ru

Abstract. Modern medical laboratory diagnostic methods often require venipuncture, which can be challenging when blood vessels are not visible to the naked eye. This potentially leads to errors in blood sampling and misinterpretation of test results. Optical methods in medicine, specifically, vein visualization in the near-infrared (NIR) range, are actively being developed. However, current methods face several limitations, including shallow imaging depth and low contrast. Additionally, digital image processing algorithms used in these methods are imperfect. These algorithms often have low stability and performance. In this study, an efficient and robust algorithm for digital image processing has been developed to enhance vein visualization. The proposed algorithm outperforms existing methods in terms of the effectiveness of separating pixels corresponding to veins from those associated with surrounding biotissues. The algorithm is based on efficient FFT-based operations.

Keywords: vein viewer; OpenCV; convolution; fast Fourier transform; Gaussian filter; ACE; Wallis filter; contrast enhancement.

Paper #9246 received 19 Feb 2025; revised manuscript received 26 Apr 2025; accepted for publication 4 May 2025; published online 28 Jun 2025. doi: 10.18287/JBPE25.11.020309.

1 Introduction

1.1 Background and Related Works

Vein viewer is a medical device used to obtain a pattern of the location of human superficial veins. The operation principle is based on the interaction of IR radiation with biological tissues (Fig. 1). The IR light, emitted in the wavelength range of 700–950 nm, passes through a diffuser. Then it penetrates the skin, illuminating a specific area of the patient's body. Hemoglobin in the blood absorbs this radiation significantly stronger than the surrounding biological tissues, which predominantly reflect the light. This differential absorption and reflection create a contrast between the blood vessels and the surrounding tissues, enabling clear visualization of the venous structure.

The reflected light is captured by a detector sensitive to the IR range, after passing through an optical filter that blocks visible light while allowing infrared light to pass through. This process generates an image that includes both the skin surface and a detailed pattern of the underlying blood vessels. The acquired image undergoes digital processing to enhance contrast. Then it is displayed on the device's LCD screen.

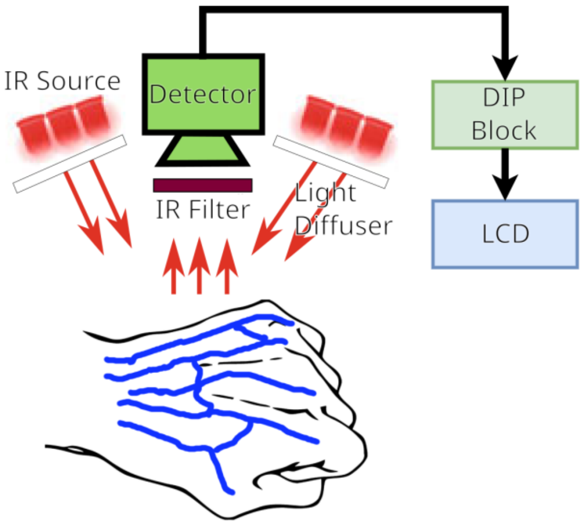

Fig. 1 Vein viewer: the main principle of method.

In medical practice, a vein viewer is a useful tool primarily used for facilitating venipuncture and supporting treatment planning. This device enhances the visibility of veins in commonly accessed areas for procedures, such as the forearm, hand, lower leg, and foot. These are common sites for catheter insertion, venipuncture, and other leg vein-related interventions, such as sclerotherapy and phlebectomy [1−3]. Beyond its clinical applications, the vein viewer also serves as an important training aid for nurses, helping them to master venous access techniques. It also aids in identifying dilated veins in patients with varicose veins, providing critical information for diagnosis and treatment.

The main limitations of near-infrared vein visualization include reduced vein visibility in certain conditions, such as skin abnormalities, dark skin tones, or excessive body weight. Also, the method is constrained by its limited imaging depth, which typically does not exceed 5 mm [1].

Thus, when diagnosing deep vein disorders, alternative techniques such as phlebography or Doppler ultrasound should be employed. However, for rapid assessment of the location of superficial veins – especially when veins are not visible to the naked eye – small, portable vein-viewing devices are preferred for venous access. NIR Vein viewer can minimize the risk of inappropriate punctures and ensure the safety of the procedure for the patient.

At present, the field of vein visualization remains insufficiently explored. Existing devices lack adequate imaging depth and lack a unified standard for device parameters. Variations exist in optical configurations, as well as in approaches to processing the acquired images [2−12]. A standardized methodology for imaging the human venous system has not yet been developed. This highlights the necessity for further research aimed at optimizing the parameters of vein visualization techniques.

The image obtained from the vein viewer in the NIR range must be digitally processed after its registration and conversion into digital form. Digital processing in the context of vein visualization addresses several tasks: noise and artifact suppression, removal of unwanted components of biological tissues (such as hair, skin defects, and background), enhancement of vein contrast relative to the skin surface, and feature segmentation for constructing a vein pattern. Due to the specific requirements of vein visualization devices, image processing must be performed in real time, which significantly complicates the development of an optimal processing algorithm.

It is important to note that the issue of image processing in the context of vein visualization remains insufficiently explored. At present, no comprehensive studies dedicated exclusively to image processing challenges in vein visualization have been found in the literature. Existing publications on vein imaging prioritize hardware, frequently neglecting image contrast enhancement procedure, with only a brief description of the methods used, or not considered at all. This highlights the need for more comprehensive investigation into this area to improve the quality and informativeness of the resulting images.

Existing researches efforts utilize approaches aimed at enhancing contrast (e.g., adaptive histogram equalization), suppressing salt-and-pepper noise (median filter), and removing background artifacts.

A. B. Abd Rahman et al. (2022) [3] describe an image processing approach that includes background removal, contrast equalization, and image smoothing. At the first stage, the GrabCut segmentation method is used to remove the background and define the boundaries of the region of interest (ROI). Then, the contrast-limited adaptive histogram equalization (CLAHE) method is applied to the ROI to enhance image contrast. Next, the Hessian segmentation method is applied to separate the vein structure from surrounding noise. This method calculates the probability of a pixel being part of a vessel. Then, median filtering is performed to suppress noise, and the inferno colormap from the Python data visualization library matplotlib is applied to the image. The use of this colormap improves human perception of the image. The algorithm gives a significant increase in the contrast of the veins relative to the skin surface. However, even when disregarding the ROI detection methods, the authors utilize computationally demanding algorithms for filtering, such as median filtering and the Hessian-based segmentation method. Furthermore, the effectiveness of the median filter is highly dependent on the window size, which ideally should be adaptively selected for each image. This requirement may impact the algorithm's robustness when dealing with variations in the capturing angle or perspective.

G. VT (2021) [4] applies a median filter to remove noise, adaptive histogram equalization to enhance contrast, binary segmentation to identify vein regions, and morphological processing to smooth the image and eliminate unwanted areas during vein visualization. The author does not provide a comprehensive mathematical description of the morphological operations used in the algorithm. While real-time operation is claimed, no evaluation of the algorithm's efficiency is presented, and the technical specifications of the equipment used are not provided. Furthermore, the methods employed are not adaptive, which may reduce the reliability of the algorithm's results. In certain cases, this limitation may necessitate manual parameter adjustment by the device operator during operation. A similar approach is proposed in the earlier studies [5, 6].

K. Ahmed et al. (2018) [7] developed an image processing algorithm that begins with the image smoothing stage. In the next step, background detection is performed to remove it and extract the ROI. After a series of transformations aimed at removing artifacts, CLAHE is applied to the extracted region to enhance image contrast. The primary method for enhancing image quality, apart from the removal of extraneous objects, is the CLAHE technique. Although it moderately improves the visibility of veins against the skin surface, the achieved effect is insufficient for the reliable extraction of fine details. A similar approach, utilizing different noise removal techniques followed by the sequential application of CLAHE, is demonstrated in Ref. [8].

M. Francis et al. (2016) [9] propose the sequential application of a median filter and a Gaussian filter to remove "salt-and-pepper" noise and smooth the image, respectively. Next, CLAHE is performed to enhance image contrast. Then, a Gabor filter is applied to improve the visibility of vein edges. Vein extraction is carried out using the Otsu thresholding algorithm. Then, an erosion operation is performed to construct the vein pattern. Then the ROI is extracted. The algorithm significantly improves image quality; however, the use of the Gabor filter and median filter introduces high computational complexity, making real-time implementation challenging on low-cost hardware.

D. Kim et al. (2017) [10] begin the image processing by extracting the ROI, followed by the application of their custom histogram equalization method. Next, the Frangi filter is applied, and segmentation is performed using an adaptive thresholding method. The authors then employ a "skeletonization" technique, which transforms the vein pattern into thin line-like structures. The algorithm effectively improves the quality of vein visualization. However, the application of the Frangi filter is characterized by high computational complexity, which may limit its applicability for real-time image processing.

N. Sharma and M. Hafeeda (2020) [11] sequentially apply CLAHE and homomorphic filtering, which suppresses low-frequency components and enhances high-frequency components of the image. Subsequently, logarithmic transformation of the image is performed. The homomorphic filtering technique is not clearly explained by authors and does not significantly enhance image contrast.

H. Ozkan et al. (2023) [12] utilize two parallel combinations of filters. In the first case, CLAHE, a median filter, and a bilateral filter are applied sequentially to the image. In the second case, the order of the smoothing filters is altered: CLAHE, followed by a bilateral filter, and then a median filter. According to the authors, this approach enables better vein enhancement in multispectral visualization. The disadvantage of the algorithm is the high computational complexity of the bilateral filter.

M. Jadhav and P. Nerkar (2015) [13] address the problem of biometric authentication, developing a method for finger vein pattern recognition based on field-programmable gate array (FPGA) device. During image processing, a fast algorithm is used, which includes a Gaussian smoothing filter followed by the Canny algorithm for edge detection. For classification, the authors employ several different feature extraction methods. The proposed digital image processing method does not allow for the estimation of vein thickness. This excludes the use of the algorithm for medical purposes.

S. Crisan et al. (2007) [14] used edge detection methods, followed by image binarization. The authors achieved a satisfactory visualization result; however, they noted the difficulty in selecting the threshold for binarization.

In studies [15−19] on the topic of visualization, the enhancement of image quality through digital processing is either not addressed or discussed only superficially.

Thus, it can be concluded that CLAHE is often used in conjunction with other methods for the processing of NIR images for vein visualization. This method is applied to enhance contrast. Various smoothing techniques are also utilized, particularly the median filter. Special algorithms are employed for edge enhancement. Additionally, background removal and ROI determination methods are actively applied.

In several studies, the CLAHE method is applied to process infrared vein images by performing local histogram equalization to enhance contrast. However, the task of vein visualization requires not only improving brightness distribution but also accurately delineating vessel boundaries. Despite this, in some algorithms, the application of a smoothing filter following CLAHE is considered sufficient. This approach may be inadequate for reliable vein segmentation due to the lack of stages specifically aimed at enhancing sharpness and suppressing noise in low-contrast regions.

As existing studies indicate, the approach to digital image processing is not directly tied to the optical configuration of the device. In other words, the operation of image processing algorithms, in most cases, does not depend on the light sources, filters, or detectors used. Regardless of the device's configuration, the same methods can be applied for digital image processing. This is because these algorithms operate at the pixel level and their intensity, independent of the characteristics of light sources or filters.

Nevertheless, the effectiveness of these algorithms indirectly depends on the quality of the original image. Image quality includes light distribution, background presence, and noise levels. These factors, in turn, may be influenced by the optical design of the device.

In several algorithms, binarization methods are employed to effectively separate veins from surrounding biotissues. However, these methods also have limitations in terms of adaptability. For instance, the application of global binarization requires threshold adjustment for each specific situation, as factors such as the imaging angle or lighting conditions may vary. These variations directly affect the image histogram and pixel distribution. The Otsu method, for example, has an inherent limitation: it performs optimally when the image histogram exhibits a bimodal distribution. Under conditions of unstable lighting and non-uniform background - which are typical for infrared vein images - the Otsu method may lead to false positives (e.g., inclusion of noisy regions) or the omission of thin vessels. Consequently, the use of binarization may complicate the practical application of the device in real-world medical settings. Moreover, adaptive binarization methods demand significantly higher computational resources.

In the reviewed studies, image processing methods characterized by high computational complexity are employed. The use of algorithms such as the Gabor filter, bilateral filter, and median filtering is demonstrated. These algorithms require significant computational resources, making them impractical for use on devices with limited performance, such as portable vein viewers. In the real-world medical practice, when image processing speed is critical, such delays can be unacceptable. This highlights the need to develop a more efficient image processing method, for example, based on the fast Fourier transform (FFT), which would combine high speed with effective visualization.

Thus, the primary objective of this study is to develop an efficient algorithm for digital processing of images obtained during vein visualization in the NIR spectrum. The algorithm must be adaptive and robust to variations in image capturing conditions. Additionally, it should be based on fast operations, ensuring low computational complexity.

This study addresses the problem of digital image processing for the visualization of venous structures. The research focuses on solving two key tasks: enhancing the contrast of the venous pattern relative to surrounding biological tissues and evaluating the effectiveness of digital filtering results. The work encompasses a comprehensive analysis of existing image processing approaches, the development of a novel algorithm to address the contrast enhancement task, and the quantitative evaluation of the obtained results.

1.2 Specifics of Image Registration in Venous Visualization

Specialized devices known as vein viewers are used to capture digital images of the human venous pattern. The quality of the resulting image is significantly influenced by the optical configuration of the device, which is determined by several key factors. These include: the spectral range of the detected light radiation, the type of light source (LED or laser diode), the shape of the light spot, the sensitivity and resolution of the detector, the characteristics of optical filters and diffusers.

It is known that the maximum penetration depth of light into biological tissues (up to 5 mm) is achieved in the near-infrared range (700−950 nm), whereas the minimum penetration depth occurs in the ultraviolet range (200−400 nm). The penetration depth is also influenced by the characteristics of the radiation source's directional pattern and the width of the light spot. Studies have demonstrated that increasing the width of the incident light spot from 1 mm to 5 mm significantly enhances the light penetration depth into biological tissues. However, starting from a spot width of 10 mm, further increases in width do not affect the penetration depth [20]. The authors attribute this phenomenon to the scattering of narrow light beams caused by the inhomogeneity of the refractive index of biological tissues. Also, the power of the radiation has a minor impact on the penetration depth, as reported in study [21].

In commercial vein viewers, both light-emitting diodes (LEDs) and laser diodes may be used as sources of light radiation. LED-based devices are simpler from a circuit design perspective, with low requirements for the driver circuitry, cooling systems, and calibration processes. However, laser-diode-based devices offer higher result reproducibility. Also, due to their ability to operate within a narrow spectral range and the use of optical filters, laser-based devices can minimize the impact of unwanted spectral components on image quality.

Optical filters must absorb visible light radiation and transmit infrared radiation in the range of 700 to 950 nm, as determined by the specific optical design of the device. The removal of background light in the visible spectrum provides greater contrast, as the radiation reflected from the upper layers of the skin does not reach the detector.

Optical diffuser is not an essential component of a vein viewer; however, its use ensures more uniform and even distribution of light radiation across the surface of biological tissue, thereby preventing overexposure in certain areas of the image. Both the geometric parameters of the diffuser and the material properties are important in this context. Thus, polycarbonate (PC) and polystyrene (PS) plastics show excellent optical properties and can be effectively used as diffusers [22, 23].

The key optical parameters of detectors that affect image quality include the type of sensor array, resolution, and spectral sensitivity. CMOS arrays generally have smaller dimensions and lower cost compared to CCD arrays. However, the architecture of CCD arrays provides higher image quality due to their superior light sensitivity and better signal-to-noise ratio (SNR). The spectral sensitivity of the array determines the range and intensity of light waves of different wavelengths detected by the sensor, which directly impacts color reproduction and overall image quality. Higher spectral sensitivity in the near-infrared (NIR) range allows for a stronger useful signal to be captured at the same exposure time. This, in turn, reduces the relative contribution of noise from the array's amplifiers in the image, thereby increasing the SNR. As a result, the array achieves high speed performance and, consequently, a higher camera frame rate.

2 Materials and Methods

The following steps were carried out during the experiment. A dataset was collected for conducting the experiment. An algorithm for digital image processing was developed using Python and OpenCV. Optimal working parameters of the algorithm were determined to achieve visually satisfactory results. An approach for evaluating the results was proposed.

The developed algorithm is characterized by the use of faster digital processing methods compared to the algorithms in the reviewed articles, which potentially allows for processing on devices with low computational power.

Most existing studies lack a clear methodology for evaluating digital filtering results. When evaluations are performed [7, 11, 12], researchers focus primarily on vessel segmentation accuracy but often neglect the impact of background (surrounding biotissues) on image quality.

We have developed a novel approach that introduces additional metrics to analyze how the background affects vein contrast and edge sharpness. By incorporating these metrics, our method significantly enhances the objectivity of result evaluation.

2.1 Dataset Compilation

The Forearm Veins dataset, consisting of 100 near-infrared (NIR) images of human forearms, was obtained through the Kaggle machine learning competition platform [24]. The creators of the dataset have not provided information about the conditions under which the data was collected.

The dataset includes forearm images with various challenges, such as poorly visible veins, tattoos, bracers, and excessive hairiness. 70 of 100 images are accompanied by vein mask annotations. Several sample images from the dataset are shown in Fig. 2, and examples of the corresponding vein masks are presented in Fig. 3.

2.2 Digital Image Processing Algorithm Development

As part of the experimental research, a comparative analysis was conducted to evaluate the effectiveness of applying the CLAHE method to the original dataset versus our custom algorithm effectiveness. We developed an algorithm that incorporates sequential application of high-frequency filtering and contrast enhancement filters.

To develop the algorithm, the Forearm Veins dataset properties were analyzed. Fig. 4 presents histograms of five images, illustrating typical parameter variations. These images were selected for their ability to demonstrate the dataset's wide parameter variability, enabling a concise visual assessment of the algorithm's robustness.

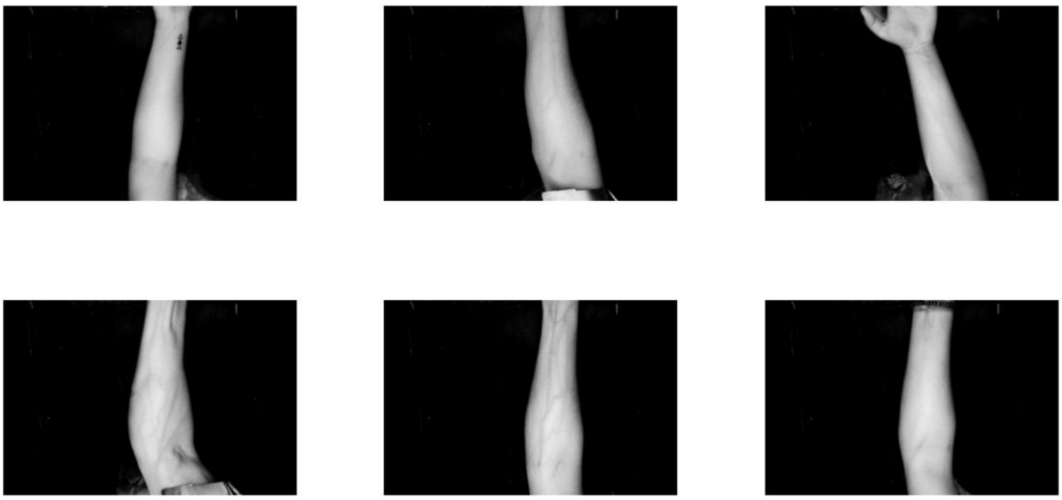

Fig. 2 Examples of images from the Forearm Veins dataset.

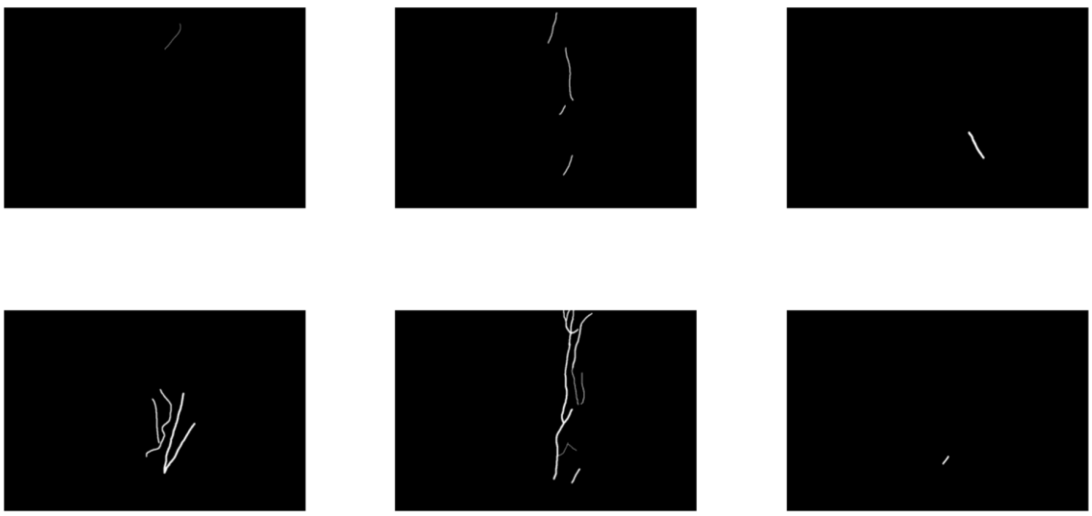

Fig. 3 Examples of vein masks from the Forearm Veins dataset.

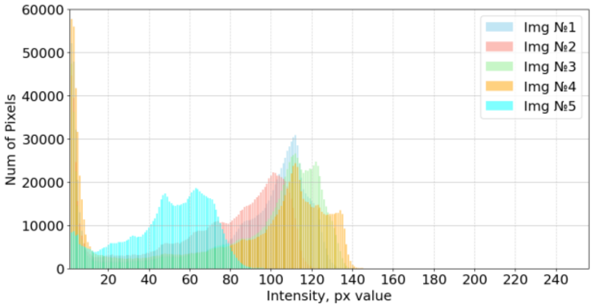

Fig. 4 Comparison of histograms of 5 images from the Forearm Veins dataset.

Fig. 5 presents the radial profiles of the spatial spectra for five images from the dataset. The radial profile is a one-dimensional slice of the two-dimensional FFT spectrum, taken along the radius at a 45° angle. This method simplifies the analysis by reducing the two-dimensional spectral data to a one-dimensional plot, avoiding the need for visual interpretation of intensities. The resulting graph shows the energy distribution across spatial frequencies: low frequencies represent large structures (e.g., background), while high frequencies correspond to fine details (e.g., vein edges).

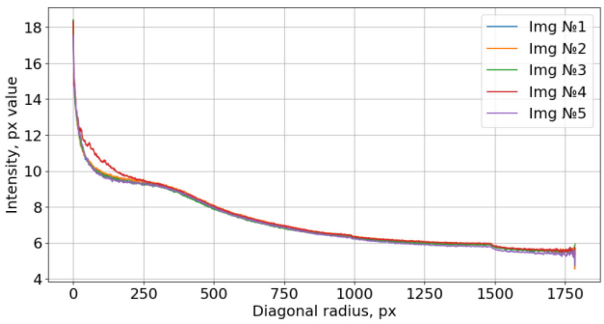

Fig. 5 Comparison of radial profiles of FFT spectra of 5 images from the Forearm Veins dataset.

The figures reveal significant differences in image histograms, with black tones dominating in all cases. However, the radial spectra profiles exhibit external similarities. An adaptive approach is suggested for histogram processing. Additionally, the similarity of spatial spectra suggests potential for applying FFT-based filters. Efficient FFT algorithms make real-time image processing feasible.

In our algorithm, a spatial high-frequency Gaussian filter is first applied to the original image. The FFT image of this filter can be calculated as follows [25]:

$$H(u,v) = 1 - exp\left(\frac{-D^2(u,v)}{2D_0^2}\right). \quad (1)$$

Following the application of the Gaussian high-pass filter (HPF), the resulting image is processed using the Adaptive Contrast Enhancement (ACE) algorithm. ACE is an adaptive image processing technique that separates the image into low-frequency and high-frequency components. The low-frequency component is determined as the local mean brightness of pixels within an $n\times n$ rectangular neighborhood (with n being odd), centered on the current pixel $x(i,j)$ [26]:

$$m_x(i,j) = \frac{1}{((2n+1)^2)} \sum_{k=i-n}^{i+n} \sum_{l=j-n}^{j+n} x\,(k,l). \quad (2)$$

The high-frequency component is calculated as the difference between the original pixel brightness value $x(i,j)$ and its local mean $m_x(i,j)$. To enhance contrast, a gain factor $G(i,j)$ is applied, which can be either constant or dependent on the local standard deviation (LSD) [26]:

$$f(i,j) = m_x(i,j) + G(i,j) \times \left(x(i,j) - m_x(i,j)\right). \quad (3)$$

A constant $G(i,j)$ may lead to ringing artifacts in the image. Consequently, the LSD is generally utilized in computations, as shown below [26]:

$$f(i,j) = m_x(i,j) + \frac{D}{\sigma_x}(i,j) \times \left(x(i,j) - m_x(i,j)\right). \quad (4)$$

where D is constant value, and LSD σ_x [26]:

$$\sigma_x^2(i,j) = \frac{1}{((2n+1)^2)} \sum_{k=i-n}^{i+n} \sum_{l=j-n}^{j+n} \left(x(k,l) - m_x(i,j)\right)^2. \quad (5)$$

The Wallis filter [27] is subsequently applied to the processed image to enhance local contrast. The Wallis filter is an adaptive method of local contrast image processing that adjusts brightness and contrast based on the statistical characteristics of each local region. Unlike global methods, which apply uniform parameters to the entire image, the Wallis filter accounts for local mean values and standard deviations. This allows it to preserve details in both low-contrast and high-contrast areas.

The filter may be implemented as follows [27]. The original image is divided into square blocks of size $n\times n$, for which local statistics are calculated - namely, the local mean $m_{original}$ and the standard deviation $s_{original}$. For each pixel in the central block, new brightness values are computed using target parameters: the desired mean m_{target} and the desired standard deviation s_{target}.

The general expression for the transformation can be written as follows [27]:

$$i_{wallis}(x,y) = i_{original}(x,y) \times r_1 + r_0. \quad (6)$$

where the coefficients r_1 and r_0 are determined by a pair of Eqs. [27]:

$$r_1 = \frac{(c \times s_{original})}{\left(c \times s_{original} + \frac{s_{target}}{c}\right)}, \quad (7)$$
$$r_0 = b \times m_{target} + (1 - b - r_1) \times m_{original}.$$

The parameter c controls the degree of contrast: small values ($c \to 0$) reduce contrast, making the image appear grayer, while values close to 1 enhance contrast. The parameter b determines the balance between target values and the original data: when $b = 1$, the output image fully matches the target parameters, whereas when $b = 0$, the original image is preserved. This filter has not been applied to vein visualization in previous researches.

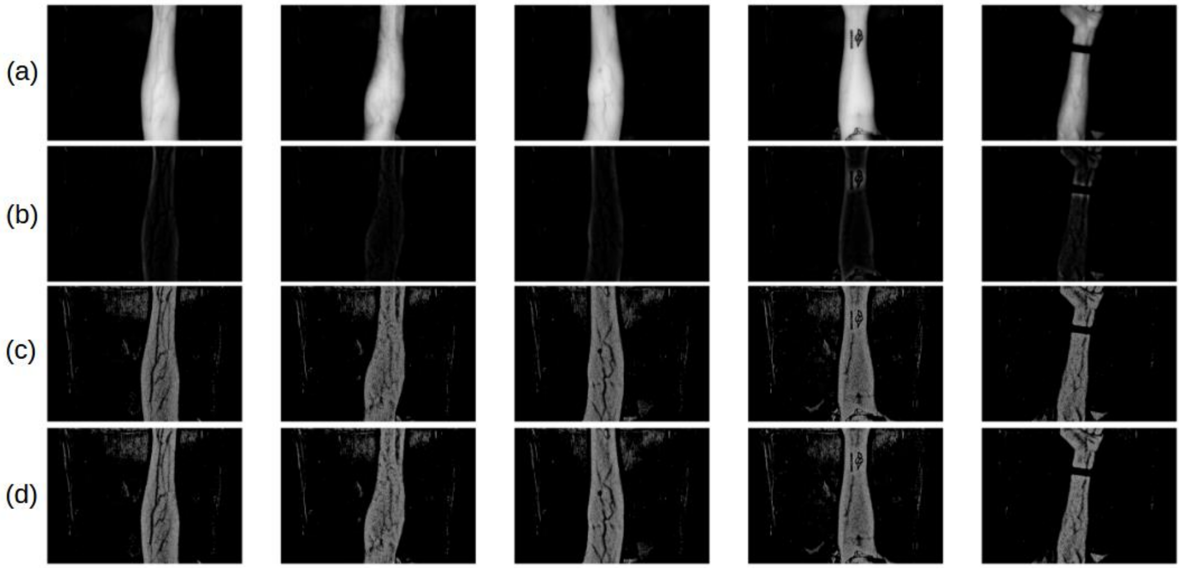

Fig. 6 A step-by-step illustration of the algorithm's operation: (a) raw image, (b) Gaussian HPF, (c) ACE, (d) Wallis filter.

However, it has proven effective in edge detection for brick walls and stained glass, tasks that are similar to vein visualization [27].

A step-by-step illustration of the algorithm's operation for five images from the original dataset is shown in Fig. 6.

The proposed algorithm effectively enhances vein contrast relative to the skin surface, as confirmed by visual analysis of the processed images: veins are clearly distinguishable in all dataset images. To the best of our knowledge, this is a novel method that not been reported in the literature previously. Furthermore, the use of optimized FFT and convolution operations from the OpenCV library ensures computational efficiency, making the algorithm suitable for deployment on low-resource devices.

2.3 Evaluation

To validate the image processing algorithms, an evaluation method was developed. The main idea behind the method is to compare the 8-bit processed images with binary reference images. The dataset includes vein mask annotations corresponding to 70 NIR digital photographs of 100. Reference images for evaluation were generated using the following procedure.

The dataset images were first processed to extract hand masks devoid of veins and background artifacts. This was achieved through automated processing using windowed rank percentile filtering. The filter aperture size was set to 65×65, enabling the smoothing of minor background artifacts.

The percentile t for filtering an image $i(x,y)$ is determined as follows:

$$t = 2 \times \frac{\sigma(x,y)}{max(x,y)}. \quad (8)$$

The general concept of the percentile filter is as follows. A sliding window moves across the image. For each window, a new value is calculated for the pixel, which corresponds to a specified percentile of the sorted pixel values within the window. For example, a percentile filter with a specified percentile of 0.5 is equivalent to a median filter.

Global threshold binarization was applied to the image, with the threshold determined as the standard deviation of the image intensity, $\sigma(x,y)$. This approach enabled the extraction of forearm masks.

A forearm mask is a binary image in which pixels corresponding to the forearm region − including veins and surrounding tissues − are assigned the maximum intensity value in grayscale representation, while all other pixels are set to zero.

Vein masks, available for 70 images in the original dataset, were subtracted from the forearm masks. This operation produced reference images in which regions corresponding to veins were set to 0. The remaining pixels represented either background or superficial tissues. The resulting reference images are presented in Fig. 7.

Two types of errors were calculated: the error in forearm processing and the error in vein processing. The root mean square error (RMSE) was evaluated for each type:

$$RMSE = \sqrt{\frac{1}{M \times N} \sum_{i=1}^{M} \sum_{j=1}^{N} \big(i(i,j) - r(i,j)\big)^2}. \quad (9)$$

Here, M denotes the image height, and N represents the image width. The terms $i(i,j)$ and $r(i,j)$ refer to the image and the reference image, respectively.

To evaluate the error associated with the forearm region, a specific area corresponding to the forearm mask is selected, excluding the vein mask region. The reference is defined as a rectangular array where all elements are equal to 255. This setup allows for assessing how closely the pixel values corresponding to the skin in the image approach the brightness value of 255.

Fig. 7 (a) Forearm masks, (b) ideal reference images.

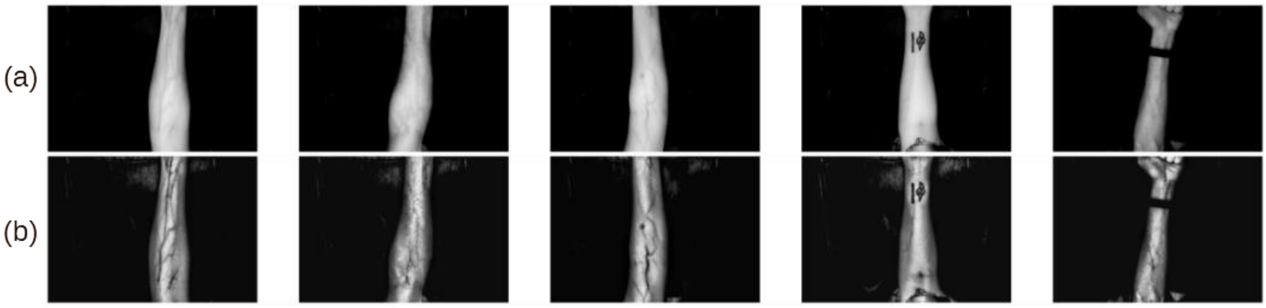

Fig. 8 Image processing with CLAHE: (a) before and (b) after.

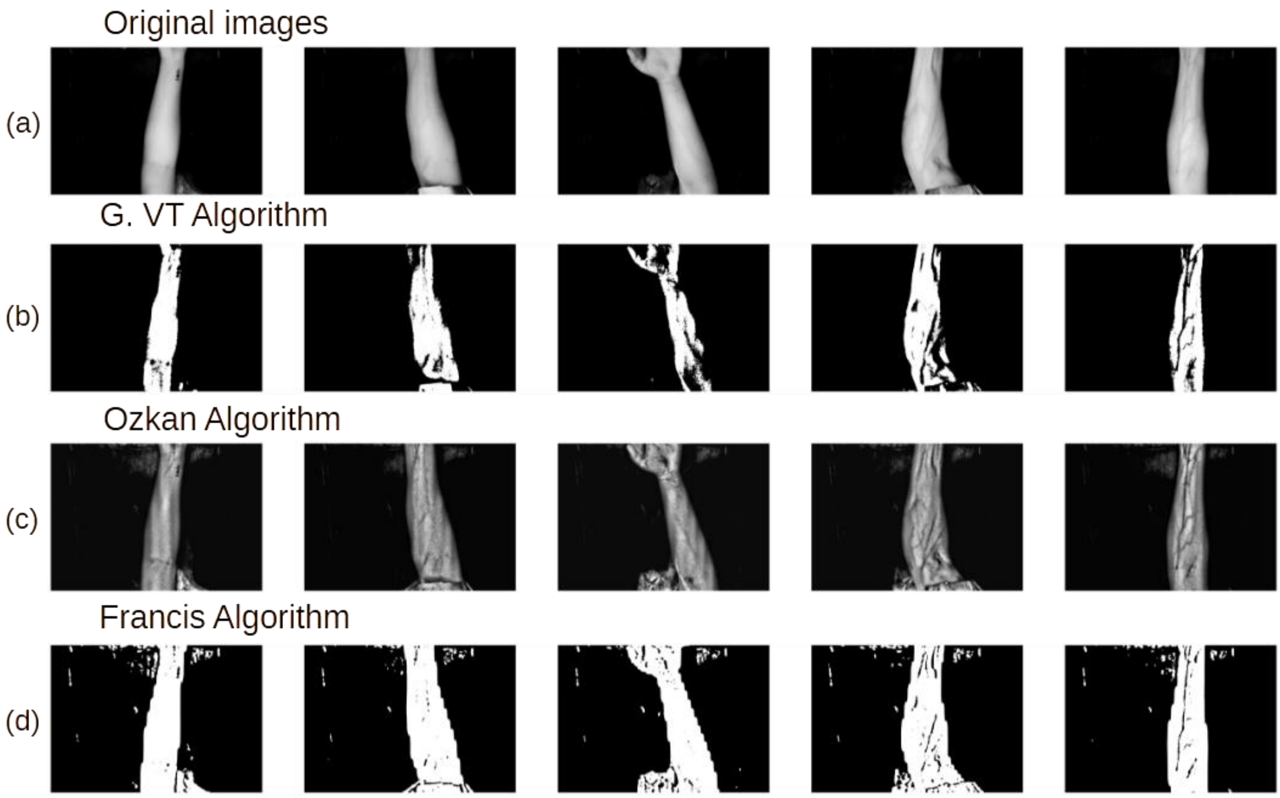

Fig. 9 (a) Original images vs (b) VT, (c) Ozkan, (d) Francis algorithms.

For evaluating the error associated with veins, the region corresponding to the veins is isolated. In this case, the reference is a rectangular array consisting entirely of zeros. This enables the assessment of how closely the pixel values corresponding to blood vessels in the image approach the brightness value of 0.

The RMSE value thus represents the root mean square deviation of the pixel values from the desired, reference ones.

To compare the efficiency of different algorithms, image processing was performed using the CLAHE algorithm was implemented separately. In general, CLAHE divides the input image into equal rectangular regions, referred as tiles. Histogram equalization is then performed for each tile. During histogram equalization, a contrast enhancement threshold is used. The main idea behind thresholding is that the number of pixels at each brightness level in the current tile's histogram should not exceed a certain predetermined value. This approach prevents excessive histogram amplification in tiles with nearly constant brightness levels. The OpenCV implementation of the algorithm also includes bilinear interpolation of the boundaries between adjacent tiles. An example of image processing using the CLAHE algorithm for five images is shown in Fig. 8.

In addition, to enable a comprehensive comparison of algorithm performance on the ForearmVeins dataset, the VT, Francis, and Ozkan algorithms [4, 9, 12] were implemented in a simplified format, excluding ROI detection methods. These algorithms were chosen due to the fact that a complete description of the processing steps is available for them. Examples of the results obtained using these algorithms are shown in the Fig. 9. The performance of these algorithms is also evaluated.

This evaluation approach was designed to provide an objective assessment of the quality of visualization. It takes into account not only the determination of vein edges but also the influence of the background. Skin and superficial tissues can significantly affect visualization. Unlike most existing studies, where result evaluation is either entirely absent or limited to analyzing vessel segmentation accuracy, the proposed approach is more versatile. It allows for simultaneous assessment of how well detected veins correspond to reference data. It also evaluates the correctness of background processing. This is particularly important because the intensity distributions of forearm areas in the original images overlap with those of vein regions. Such overlap directly impacts the quality of visualization and image processing requirements. The developed algorithm addresses this issue. It allows to identify a clear boundary on the histogram between regions corresponding to veins and those belonging to surrounding biological tissues.

3 Results and Discussion

The following results were obtained during the experiment. The developed algorithm achieves a significant reduction in pixel brightness error for veins. However, it slightly increases the pixel brightness error for skin areas. These effects are illustrated in Figs. 10 and 11.

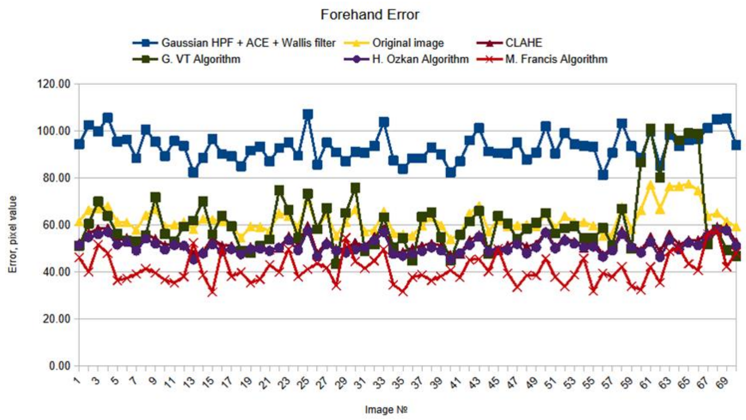

Fig. 10 Comparison of skin brightness error for five cases: without preprocessing, with preprocessing using the developed algorithm (Gaussian HPF + ACE + Wallis filter), with CLAHE, and with the methods proposed by Francis, Ozkan, and VT.

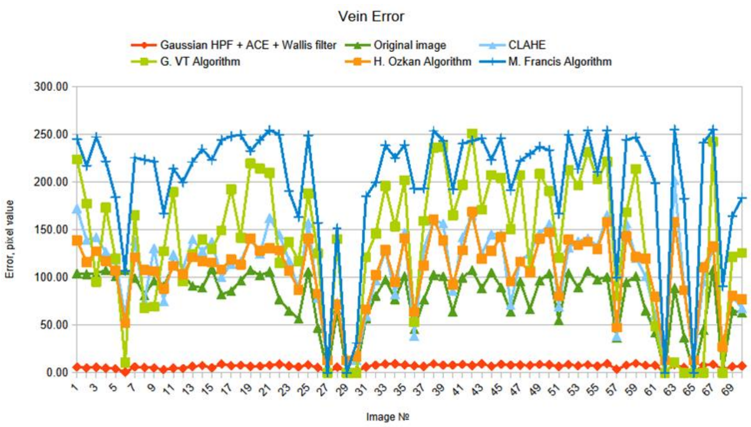

Fig. 11 Comparison of vein darkness error for five cases: without preprocessing, with preprocessing using the developed algorithm (Gaussian HPF + ACE + Wallis filter), with CLAHE, and with the methods proposed by Francis, Ozkan, and VT.

Pixel brightness error for skin areas is defined as the RMSE (Eq. (9)) calculated for pixels belonging to the skin area on the forearm, excluding regions corresponding to veins and background. The reference brightness level is set to 255, which represents the maximum possible value for an 8-bit image.

Pixel brightness error for veins is defined as the RMSE (Eq. (9)) calculated for pixels belonging to the vein area on the forearm, excluding regions corresponding to skin and background. The reference brightness level is set to 0, which represents the minimum possible value for an 8-bit image.

These definitions imply that the RMSE metric serves as a measure of how closely the pixel values align with the target reference levels for 8-bit image. Specifically, the RMSE value thus represents the root mean square deviation of the pixel values from the desired, reference ones.

All results are presented graphically to ensure clarity. In these graphs:

- The x-axis corresponds to the image number from the ForearmVeins dataset.
- The y-axis represents the error estimate.

This graphical representation offers a clearer and more intuitive interpretation than tabular data representation.

The results from the figures demonstrate the following:

- The vein darkness error for all images, after preprocessing using the developed algorithm, is close to 0.
- The skin brightness error increased from an average of 62 to an average of 93 (with preprocessing).

Key considerations regarding pixel values are as follows. Vein pixel brightness should ideally be close to 0, while skin pixel brightness should ideally approach 255. However, even if skin pixel brightness values are significantly lower than 255, human perception of the images is unlikely to be impaired. Taking this into account, the developed algorithm significantly enhances vein visualization efficiency. Furthermore, the processed images show more uniform pixel distribution compared to both the original images and those processed using CLAHE.

After processing the images using the developed algorithm, the forearm veins images' histograms converged to a more uniform shape. The histograms of all images were found to be right-skewed, with a uniform range of intensity values. A significantly larger number of pixels now have a value of zero. This makes it easier to differentiate veins from skin, as most vein pixels now correspond to a value of 0. In the original images, vein brightness varied widely, complicating the differentiation between veins and skin. The uniformity of the histograms allows for simple calculations to adjust the overall image brightness.

Visual analysis and RMSE evaluation reveal the following. The developed algorithm effectively separates pixels corresponding to veins from those representing the forearm. The deviation of vein-associated pixels from zero is minimal, indicating stable vein detection, as confirmed by the graphs (Figs. 8, 10). By normalizing vein-associated pixels to a single level, the algorithm solves the problem of vein detection and simplifies subsequent automatic segmentation, if required.

Algorithms including binarization methods (VT, Francis) demonstrate generally unstable results. As shown in Fig. 8, vein error values can vary significantly, ranging from 75 pixel values (excluding images with very few vein-associated regions) to 250 for both the VT and Francis algorithms. In contrast, the error for the forearm region remains stable for both algorithms, as shown in Fig. 7. Due to the manual threshold selection, visualization quality varies significantly across different images. Additionally, the presence of a dark background adversely affects the performance of the Francis algorithm. While the article reports satisfactory visualization quality, quantitative metrics are not particularly informative in this case. This is because the resulting 8-bit images have only two brightness levels: 0 and 255 pixel values. Quantitative evaluation primarily highlights the high likelihood of incorrect pixel classification during binarization, as evidenced by the large errors observed in the graphs. In this case, for the given dataset, the obtained results indicate low reliability of the visualization outcomes, with a significant number of incorrectly classified pixels during binarization. This implies that the automation of image processing using these methods is challenging.

The application of CLAHE, as well as the Ozkan algorithm enhanced with bilateral and median filtering, visually improves image quality. However, these methods fail to provide reliable separation of pixel groups, as show in Figs. 7, 8. Specifically, vein brightness does not approach zero, indicating no significant improvement in image contrast. The application of CLAHE does not ensure that veins will appear perfectly black if their original brightness overlaps with the background. Consequently, no effective image segmentation occurs.

In the original images, the pixel levels corresponding to veins overlap with those of the surrounding biotissues. Moreover, the brightness range of the vein pixels on the histogram may be in an unpredictable range. A similar situation was observed when processing with the Ozkan algorithm. However, for the developed algorithm, the majority of vein-associated pixel levels are reduced to zero, while the mode of the pixel level for surrounding biotissues is located around 9–10.

On the other hand, the developed algorithm, based on the Gaussian high-pass filter, slightly increases the error for skin areas but significantly reduces the error for veins, in comparison with original image. This results in higher-contrast images, enabling clear differentiation between the background and veins.

Furthermore, developed algorithm can be efficiently implemented using fast convolution techniques and FFT. It shows strong potential for real-time applications.

The developed image processing algorithm for vein visualization potentially demonstrates high efficiency in specialized medical applications, such as supporting intravenous injections and preoperative planning for phlebectomy. Notably, the algorithm consistently achieves excellent results on the current dataset, correctly processing all provided forearm images. However, it is important to consider that this method has been tested only on a limited sample, primarily using data obtained from patient forearms. This imposes certain limitations on its applicability to other body parts, where anatomical features and imaging conditions may differ significantly.

In real clinical settings, the algorithm may face additional challenges not accounted for in this study, such as variations in lighting, skin types, or patient movements. To address these limitations, two main directions for further development are proposed: first, expanding the dataset size to cover a broader range of clinical cases, and second, integrating the algorithm into actual medical devices for long-term practical testing. This approach will not only verify the system's reliability under real-world conditions but also enable the collection of valuable data for subsequent algorithm improvements.

4 Conclusion

This work presents an efficient digital image processing algorithm designed to improve the visualization quality of subcutaneous veins in the near-infrared spectrum. The proposed method significantly enhances the contrast between veins and surrounding tissues, which is essential for accurate and reliable visualization.

To evaluate the algorithm's performance, a quantitative assessment method was proposed. The developed algorithm reduces vein brightness error by 20−40% compared to the original images. After processing, the brightness of vein-related pixels approaches 0, significantly simplifying their differentiation from skin areas. This is confirmed both by numerical metrics and visual analysis of the images.

The error for skin areas increases by 10−15%. However, this change remains acceptable because it does not impair human perception of the image. Moreover, the histograms of the processed images converge to a uniform shape, enabling simple brightness transformations to be applied to the image.

Comparison with the CLAHE algorithm, widely used in vein visualization studies, highlights the superiority of the developed algorithm. While CLAHE increases vein error by 10−40% and reduces skin error only marginally (5−10%), the proposed algorithm achieves better differentiation between veins and the background. This improvement is made possible by applying Gaussian high-pass filtering, which effectively enhances fine details.

A comparative analysis with other algorithms has been performed. The developed algorithm demonstrates superior performance in terms of robustness, adaptability, and efficiency of pixel separation. Furthermore, the developed algorithm effectively reduces the brightness of most pixels related to veins to zero. This allows for reliable segmentation of pixels related to veins from pixels related to surrounding biological tissues. This differentiates developed algorithm from most other existing algorithms in a beneficial way.

The algorithm is expected to perform well due to the use of fast convolution techniques and the Fast Fourier Transform, which are implemented in OpenCV. This makes it potentially suitable for real-time image processing, which is a critical requirement in clinical settings such as venipuncture and blood sampling procedures.

Disclosures

All authors declare that there is no conflict of interest in this paper.

References

1. N. V. Remizov, E. M. Bataeva, D. P. Stramousov, A. A. Shatskaya, and D. N. Artemyev, "3D printed modular vein viewing system based on differential light absorption in the near infrared range," Journal of Biomedical Photonics & Engineering 9(2), 020307 (2023).
2. M. D. Francisco, W.-F. Chen, C.-T. Pan, M.-C. Lin, Z.-H. Wen, C.-F. Liao, and Y.-L. Shiue, "Competitive real-time near infrared (nir) vein finder imaging device to improve peripheral subcutaneous vein selection in venipuncture for clinical laboratory testing," Micromachines 12(4), 373 (2021).
3. A. B. Abd Rahman, F. Juhim, F. P. Chee, A. Bade, and F. Kadir, "Near infrared illumination optimization for vein detection: hardware and software approaches," Applied Sciences 12(21), 11173 (2022).
4. G. Vt, "A novel design proposal for low-cost vein-viewer for medical and non-contact biometric applications using NIR imaging," Journal of Medical Engineering & Technology 45(4), 303–312 (2021).
5. M. Mansoor, S. N. Sravani, S. Z. Naqvi, I. Badshah, and M. Saleem, "Real-time low cost infrared vein imaging system," in Image Processing & Pattern Recognition 2013 International Conference on Signal Processing, 117–121 (2013).
6. M. Z. Yildiz, Ö. F. Boyraz, "Development of a low-cost microcomputer based vein imaging system," Infrared Physics & Technology 98, 27–35 (2019).
7. K. I. Ahmed, M. H. Habaebi, and M. R. Islam, "A real time vein detection system," Indonesian Journal of Electrical Engineering and Computer Science 10(1), 129–137 (2018).
8. S. Naik, R. Phadnis, and M. Prabhu, "Real time vein detection and mapping using near infra-red lights," in 2020 IEEE 17th India Council International Conference, 1–6 (2020).

9. M. Francis, A. Jose, G. Devadhas, K. K. Avinashe, "A novel technique for forearm blood vein detection and enhancement," Biomedical Research 28(1), 2913–2919 (2017).
10. D. Kim, Y. Kim, S. Yoon, and D. Lee, "Preliminary study for designing a novel vein-visualizing device," Sensors 17(2), 304 (2017).
11. N. Sharma, M. Hafeeda, "Hyperspectral reconstruction from RGB images for vein visualization," Proceedings of the 11th ACM Multimedia Systems Conference (ACM, 2020), 77–87 (2020).
12. H. Ozkan, M. Aydin, O. A. Ozcan, and U. Zengin, "A portable multispectral vein imaging system," Journal of Electrical Engineering 74(1), 64–69 (2023).
13. M. Jadhav, P. M. Nerkar, "FPGA-based finger vein recognition system for personal verification," International Journal of Engineering Research and General Science 3(4), 382–388 (2015).
14. S. Crisan, J. G. Tarnovan, and T. E. Crisan, "A low cost vein detection system using near infrared radiation," 2007 IEEE Sensors Applications Symposium, 1–6 (2007).
15. F. Wang, A. Behrooz, M. Morris, and A. Adibi, "High-contrast subcutaneous vein detection and localization using multispectral imaging," Journal of Biomedical Optics 18(5), 050504 (2013).
16. H. Y. May, F. Ernawan, "Real time vein visualization using near-infrared imaging," 2020 International Conference on Computational Intelligence, 276–280 (2020).
17. M. Hamza, R. Skidanov, and V. Podlipnov, "Visualization of subcutaneous blood vessels based on hyperspectral imaging and three-wavelength index images," Sensors 23(21), 8895 (2023).
18. J. H. Song, C. Kim, and Y. Yoo, "Vein visualization using a smart phone with multispectral wiener estimation for point-of-care applications," IEEE Journal of Biomedical and Health Informatics 19(2), 773–778 (2015).
19. J. E. S. Pascual, J. Uriarte-Antonio, R. Sanchez-Reillo, and M. G. Lorenz, "Capturing hand or wrist vein images for biometric authentication using low-cost devices," in 2010 Sixth International Conference on Intelligent Information Hiding and Multimedia Signal Processing, 318–322 (2010).
20. C. Ash, M. Dubec, K. Donne, and T. Bashford, "Effect of wavelength and beam width on penetration in light-tissue interaction using computational methods," Lasers in Medical Science 32(8), 1909–1918 (2017).
21. I. Ahmed, A. Bykov, A. Popov, I. Meglinski, and M. Katz, "Optical wireless data transfer through biotissues: practical evidence and initial results," BODYNETS 2019 – 14th EAI International Conference on Body Area Networks: Smart IoT and big data for intelligent health management, 191–205 (2019).
22. N. Song, X. Hou, S. Cui, C. Ba, D. Jiao, P. Ding, and L. Shi, "Polycarbonate composites: Effect of filler type and melt-blending process on the light diffusion properties," Polymer Engineering and Science 57(4), 374–380 (2017).
23. J.-W. Huang, Y.-M. Kao, P.-W. Chiu, T.-H. Wu, and Y.-C. Lee, "Light diffusion film fabricated using colloidal lithography and embossing," Journal of Nanoparticle Research 23(1), 25 (2021).
24. C. M. Nugent, Forearm Veins (NIR) Dataset, Kaggle (accessed 20 January 2025). [https://www.kaggle.com/datasets/chrismnugent/forearm-veins-nir].
25. R. C. Gonzalez, R. E. Woods, Digital Image Processing, 3rd ed., Prentice Hall, New Jersey (2008). ISBN: 978-0-13-505267-9.
26. D.-C. Chang, W.-R. Wu, "Image contrast enhancement based on a histogram transformation of local standard deviation," IEEE Transactions on Medical Imaging 17(4), 518–531 (1998).
27. M. Jazayeri, C. Fraser, "Interest operators in close-range object reconstruction," The International Archives of the Photogrammetry, Remote Sensing and Spatial Information Sciences 37, 69–74 (2008).